The Astrophysical Journal Supplement Series, 229:5 (10pp), 2017 March https://doi.org/10.3847/1538-4365/229/1/5

Photospheric Response to an Ellerman Bomb-like Event—An Analogy of SUNRISE/IMaX Observations and MHD Simulations

S. Danilovic[1], S. K. Solanki[1,2], P. Barthol[1], A. Gandorfer[1], L. Gizon[1,3], J. Hirzberger[1], T. L. Riethmüller[1], M. van Noort[1], J. Blanco Rodríguez[4], J. C. Del Toro Iniesta[5], D. Orozco Suárez[5], W. Schmidt[6], V. Martínez Pillet[7], and M. Knölker[8,9]
[1] Max-Planck-Institut für Sonnensystemforschung, Justus-von-Liebig-Weg 3, D-37077 Göttingen, Germany; danilovic@mps.mpg.de
[2] School of Space Research, Kyung Hee University, Yongin, Gyeonggi, 446-701, Korea
[3] Institut für Astrophysik, Georg-August-Universität Göttingen, Friedrich-Hund-Platz 1, D-37077 Göttingen, Germany
[4] Grupo de Astronomía y Ciencias del Espacio, Universidad de Valencia, E-46980 Paterna, Valencia, Spain
[5] Instituto de Astrofísica de Andalucía (CSIC), Apartado de Correos 3004, E-18080 Granada, Spain
[6] Kiepenheuer-Institut für Sonnenphysik, Schöneckstr. 6, D-79104 Freiburg, Germany
[7] National Solar Observatory, 3665 Discovery Drive, Boulder, CO 80303, USA
[8] High Altitude Observatory, National Center for Atmospheric Research, P.O. Box 3000, Boulder, CO 80307-3000, USA
Received 2016 July 20; revised 2016 September 13; accepted 2016 October 24; published 2017 March 22

Abstract

Ellerman Bombs are signatures of magnetic reconnection, which is an important physical process in the solar atmosphere. How and where they occur is a subject of debate. In this paper, we analyze SUNRISE/IMaX data, along with 3D MHD simulations that aim to reproduce the exact scenario proposed for the formation of these features. Although the observed event seems to be more dynamic and violent than the simulated one, simulations clearly confirm the basic scenario for the production of EBs. The simulations also reveal the full complexity of the underlying process. The simulated observations show that the Fe I 525.02 nm line gives no information on the height where reconnection takes place. It can only give clues about the heating in the aftermath of the reconnection. However, the information on the magnetic field vector and velocity at this spatial resolution is extremely valuable because it shows what numerical models miss and how they can be improved.

Key words: Sun: activity – Sun: magnetic fields – Sun: photosphere – techniques: photometric

1. Introduction

Magnetic reconnection is an important physical processes that has a major effect on the energy budget of the solar atmosphere. It is a mechanism behind a myriad of dynamic atmospheric phenomena, ranging from small-scale flux cancellation in the solar photosphere to the largest solar disruptions—i.e., flares.

Recently, a number of studies have concentrated on explaining one of these phenomena, called the Ellerman Bomb (EB; Ellerman 1917) that poses a considerable challenge to models because of its specific characteristics. Ellerman Bombs are defined as transient brightenings of the extended wings of the Hα line, but leave signatures also in Ca II H and Ca II IR 854 nm (Vissers et al. 2013; Rezaei & Beck 2015), and sometimes even in observables that should sample temperatures orders of magnitude higher than the former (Vissers et al. 2015; Tian et al. 2016). Observations show that EBs are almost exclusively formed in young, emerging, active regions, usually between spots/pores where the emergence of serpentine field lines takes place. Series of EBs usually appear aligned along the orientation of the active region, in so-called Bald Patches (BPs)—dips in magnetic field lines (Pariat et al. 2004, 2006). This scenario is also supported by MHD simulations (Isobe et al. 2007; Archontis & Hood 2009).

Because EBs assume the shape of a flame that seems to be rooted in the intergranular lanes (Matsumoto et al. 2008; Hashimoto et al. 2010; Watanabe et al. 2011), it has been suggested that their formation begins very low, near the surface. However, one- and two-dimensional modeling strongly suggests that only a temperature increase starting at heights of a few hundred km above the solar surface can produce the observed Hα line profile without continuum brightening (Kitai 1983; Fang et al. 2006; Bello González et al. 2013; Berlicki & Heinzel 2014; Hong et al. 2014). Nelson et al. (2013) analyzed observations along with similar events in 3D MHD simulations, and inferred that EBs occur co-spatially with regions of strong opposite-polarity magnetic field at locations where the Fe I 630.25 nm line core intensity increases. According to them, this gives enough evidence that EBs are, in fact, signatures of photospheric magnetic reconnection. Later, it was established that most of the features observed by Nelson et al. (2013) were actually "pseudo-EBs," that were merely strong-field magnetic concentrations (Rutten et al. 2013). Reid et al. (2016) imposed a more discriminating threshold for detecting EBs, and corrected the previously made mistake. Their detailed analysis of a large number of these features goes beyond simply looking at the Fe I 630.25 nm line's core intensity. Using inversions of the spectropolarimetric data, they retrieved temperature enhancements of 200 K at the EBs' footpoints. This value is below the lowest number required by Hα line modeling. Reid et al. (2016) attributed this to the low formation height of Fe I 630.25 nm line.

In this paper, we analyze the photospheric response to an EB observed by the Imaging Magnetograph eXperiment (IMaX, Martínez Pillet et al. 2011) on board SUNRISE, a balloon-borne solar observatory (Solanki et al. 2010; Barthol et al. 2011; Berkefeld et al. 2011; Gandorfer et al. 2011). Similar to Nelson et al. (2013), we compare the observations with MHD simulations. However, unlike them, we carry out an appropriate numerical experiment. Whereas they used a run where cancellation of weak network was simulated, we reproduce the exact scenario proposed for the formation of EBs, i.e., the emergence of serpentine magnetic flux.

[9] The National Center for Atmospheric Research is sponsored by the National Science Foundation.

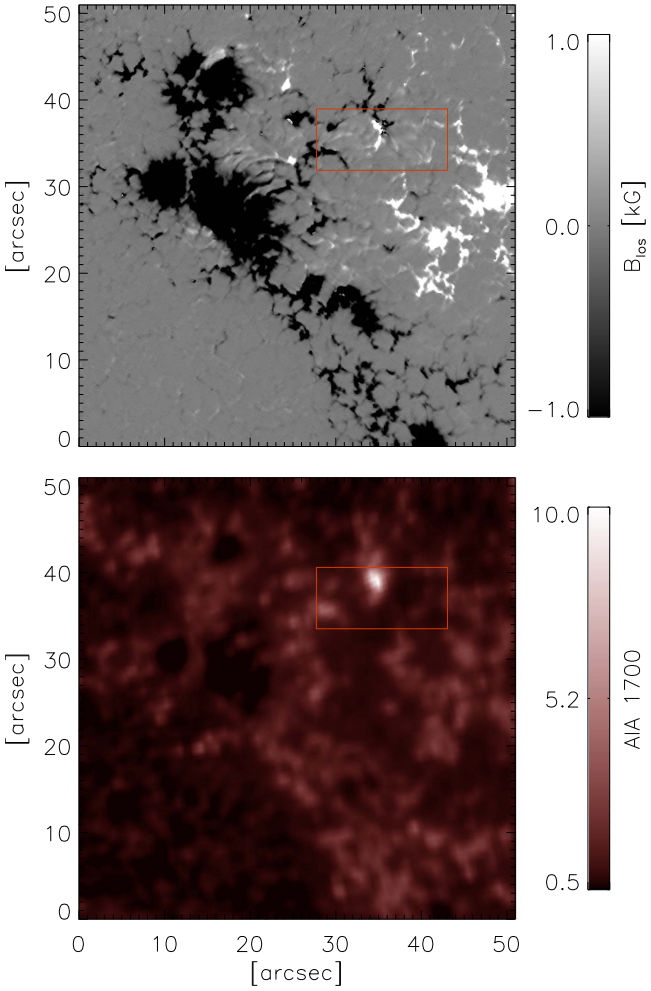

Figure 1. Line-of-sight magnetic field (top) over the whole FOV of SUNRISE/IMaX and the corresponding AIA 1700 channel image (bottom) on 2013 June 12th at 23:47 UT when the event reached its highest brightness. The red rectangle outlines the subfield shown in Figures 2 and 3. The FOV is inverted relative to that in Solanki et al. (2017), where the true orientation on the Sun is shown.

Furthermore, we take into account the spectral and spatial resolution of our instrument, as well as its polarimetric sensitivity, and apply the same inversion strategy as in the case of the observations. We pinpoint possible errors that this kind of analysis could produce, and finally show which characteristics of EBs numerical simulations fail to reproduce and why.

2. An Event Observed by SUNRISE II

The investigated event appeared during the second flight of SUNRISE (Solanki et al. 2017), in the young and growing region NOAA AR 11768 on 2013 June 12th at 23:40 UT, when the AR was located at $\mu = 0.93$. Figure 1 shows the full field of view (FOV) of the SUNRISE/IMaX instrument and the corresponding image recorded in the SDO/AIA 1700 channel (Lemen et al. 2012; Pesnell et al. 2012) when the event reached its highest brightness at 23:47 UT. Centeno et al. (2017) described, in detail, the flux emergence that led to its onset and its chromospheric signatures seen by the SUNRISE Filter Imager (SuFI; Gandorfer et al. 2011), the other instrument on board SUNRISE. We concentrate only on the photosphere; in particular, the SUNRISE/IMaX data that continuously recorded the evolution of emerging magnetic field from approximately two minutes before the appearance of the event until its extended decay some 15 minutes after. Figures 2 and 3 show the results of the 1D version of the SPINOR inversion code (Frutiger et al. 2000) applied to the data (Solanki et al. 2017) at five instances of time.[10] The inversion strategy allows temperature to be modified at three nodes along the line of sight (LOS), whereas the magnetic field vector and LOS velocity are assumed to be constant with height.

SUNRISE/IMaX time series start shortly after the footpoints of the second emerging loop appear (Centeno et al. 2017). Inverted maps of LOS velocity show fast upflows already at the beginning of the time series, and they seem to continue for over seven minutes. During that period, the spatial extent of the upflowing region increases from 2″ to approximately 6″, and the maximum projected LOS velocity exceeds 4 km s^{-1}. The emergence is, however, not symmetric. Faster upflows appear near the negative footpoint, which is also more concentrated and moves much faster than the positive one. It approaches the previously formed opposite polarity, i.e., the positive footpoint of the other emerging event, with a projected horizontal speed of approximately 3.5 km s^{-1}. Once it comes into contact with pre-existing magnetic features, the brightness in the AIA 1700 channel starts to increase. The brightness in the AIA 1700 channel reaches its maximum almost at the same time when upflows cease. It then gradually fades, but it does not dim completely; the two opposite polarities are still visible at the end of the SUNRISE/IMaX time series.

During the emergence and cancellation, a temperature increase is detected at several locations. Two are particularly interesting because we find counterparts in simulations: at the negative polarity footpoint, and the neutral line between the two polarities. The region that coincides with the negative polarity footpoint of the emerging system shows a temperature increase very early on, at the beginning of the emergence ([11″, 5″] at t = 23:40:59 UT, top panels in Figures 2 and 3). There, at all instances, the inversion code returns increased temperature at all nodes. At first, the temperature rises by less than 50 K at all three levels, but it increases by more than 1000 K at the lowest and more than 1500 K at the highest node when the footpoint reaches the opposite polarity (t = 23:44:38 UT). At the second location of interest, the neutral line between the opposite polarities, the code returns the temperature increase at the highest node first (t = 23:44:38 UT), and only in the next frame (i.e., 36.5 s later) is the temperature jump also retrieved at the lower nodes. At this region, the highest temperature increase again does not go over 1500 K, and is largest at the highest node.

3. A Simulated Event

We focus on one of the simulated events produced in the numerical experiment performed with the 3D MHD MURaM code (Vögler et al. 2005; Rempel et al. 2009). The simulation domain extends over 12 × 6 × 3.5 Mm, of which 2 Mm is above the surface. The horizontal and vertical grid spacings are 11 and 14 km, respectively. In this run, a thin flux sheet is introduced in fully developed convecting flow, some 300 km below optical depth unity. The field strength across the sheet changes as a Gaussian function with FWHM = 50 km, and

[10] The whole evolution can be found at http://www2.mps.mpg.de/data/outgoing/danilovic/ebs/.

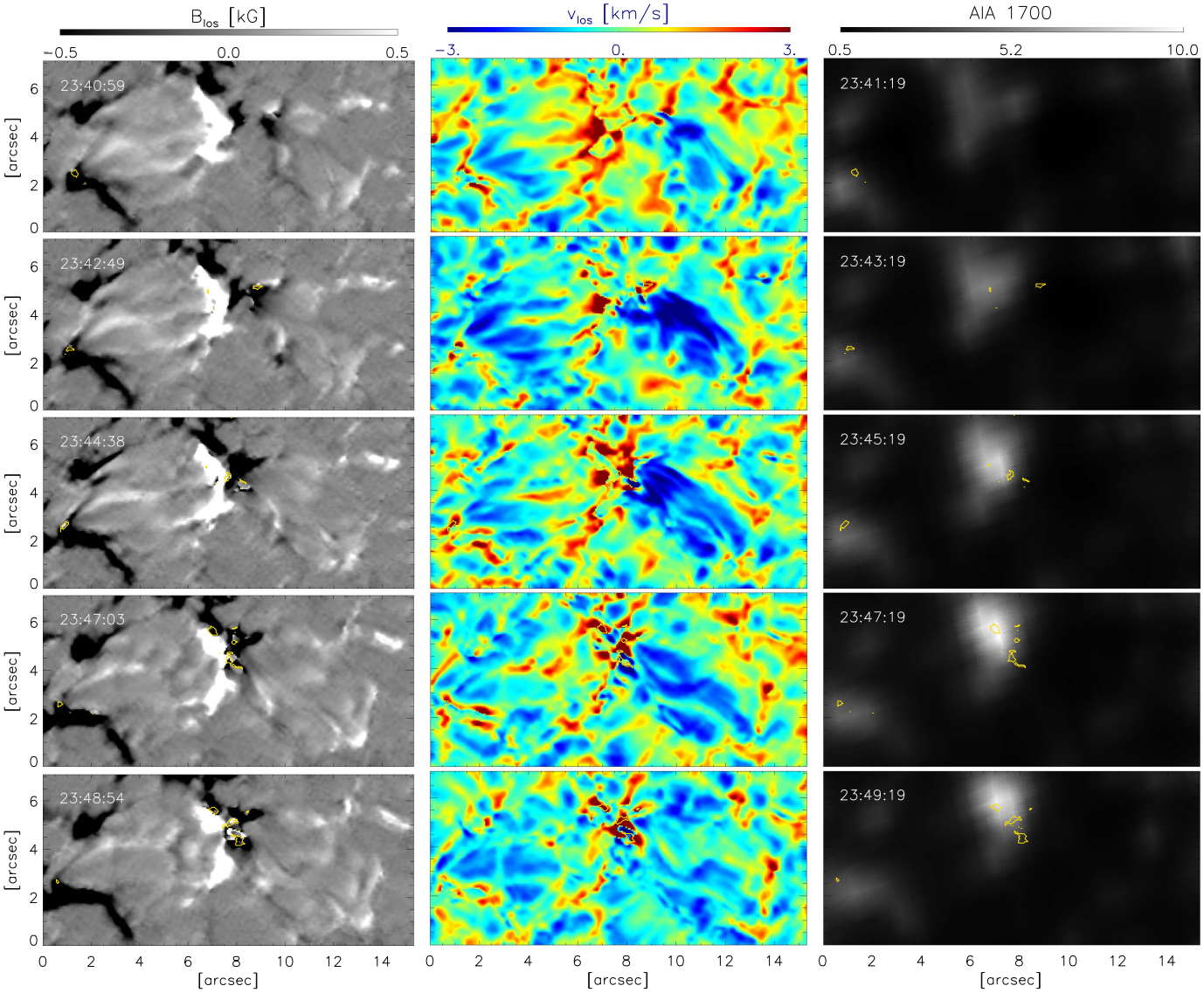

Figure 2. A small FOV around the observed event—Left and middle columns show the evolution of the LOS magnetic field and LOS velocity obtained from the inversions at five instances of time. Corresponding AIA 1700 channel images are given in the right column. Yellow contours mark the position where the temperature returned by the inversion at $\log\tau = -2.5$ exceeds 5400 K.

reaches a maximum value of 5000 G. The sheet gets undulated due to convection in such a way that crests/troughs are formed where convective upflows/downflows are present. In this way, a serpentine type of emergence develops. Figure 4 shows the field topology at two moments during the evolution of the chosen event. The top panel shows the moment when the EB is triggered, i.e., signatures appeared in the blue wing of Hα ($t = 17.5$ minute). Although the loop system already at that point reached the highest layers of the simulation box, the reconnection happened lower. Extended U-loops expanded from the reconnection site to the top of the box, with their troughs moving quickly upward due to magnetic tension. At $t = 25.8$ minute (bottom panel in Figure 4), the current sheet extended upward as more material arrived at those heights and BPs were situated far from the photosphere.

To simulate SUNRISE/IMaX observations, we synthesize the Fe I 525.02 nm line by taking into account spectral resolution and sampling of the instrument. Because we compare with reconstructed data that are approximately corrected for stray light, we remove only the spatial frequencies above the diffraction limit of the telescope from the simulated maps and rebin them to pixel size of $0\farcs055$. Noise of $7 \cdot 10^{-3}\ I_c$ is added to the simulated spectropolarimetric signals, and then the same inversion strategy is applied as for the observations. Results of the inversions are shown in Figures 5 and 6.[11]

Figure 5 also shows the simulated blue wing of Hα in the rightmost column, so that the regions where EB-like events appear may be distinguished. Emergent Hα-wing intensity is calculated with the SPINOR code in LTE, which is an acceptable assumption for the line wings (Leenaarts et al. 2006). We also add linear Stark broadening as prescribed by Rutten (2016). The figures correspond to $\mu = 0.66$, instead of the $\mu = 0.93$ of the observations, to create more pronounced flame-like shapes. These images are not spatially degraded. The

[11] A movie with the maps of parameters deduced from the inversion of the whole simulated time series is available at http://www2.mps.mpg.de/data/outgoing/danilovic/ebs/.

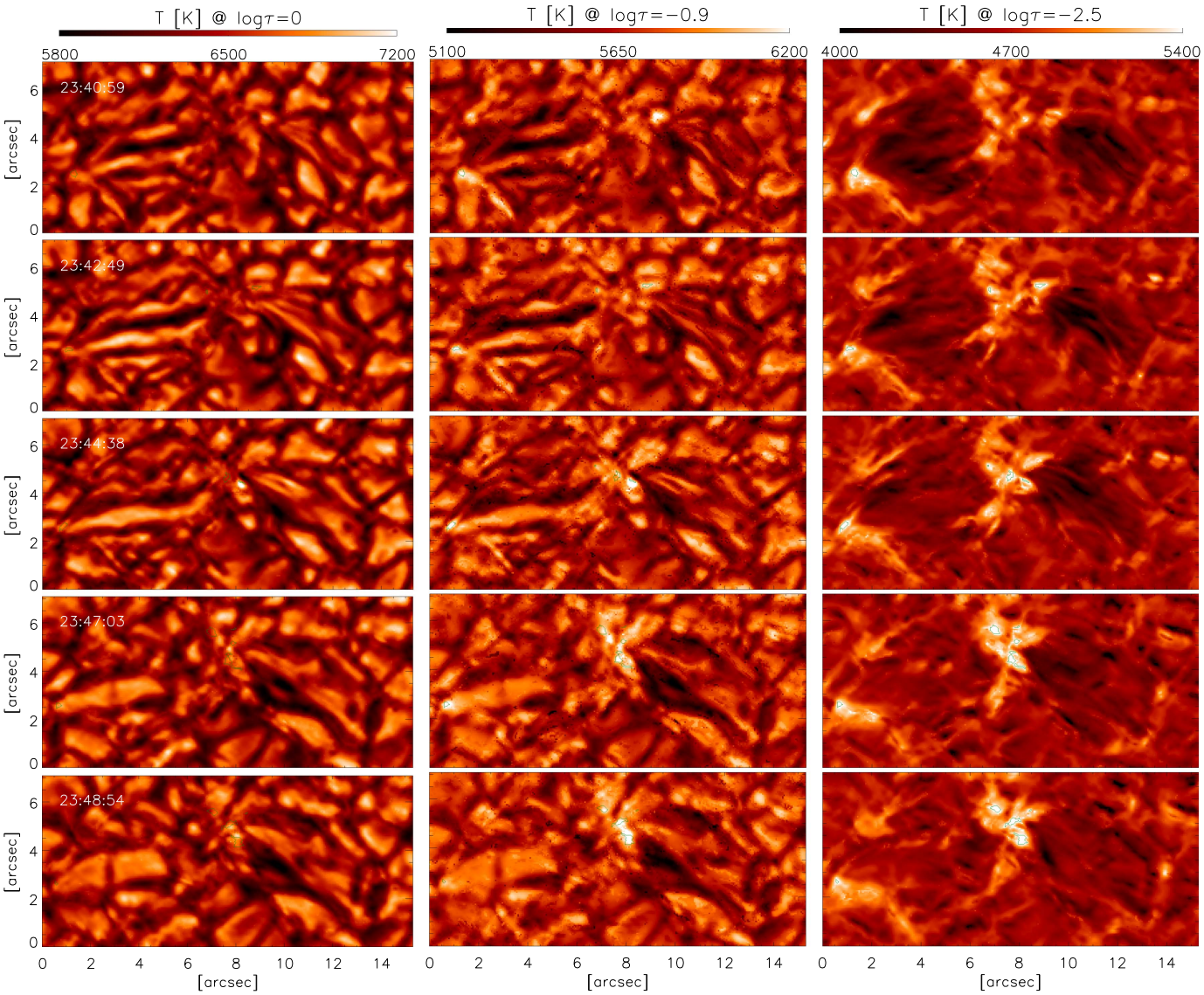

Figure 3. Maps of parameters obtained from inversions of the SUNRISE/IMaX observations—left to right: temperatures at $\log\tau = 0$, -0.9 and -2.5 at the same times as in Figure 2. Green contours mark the position where the temperature at $\log\tau = -2.5$ exceeds 5400 K.

flame that appears in the middle of the images is the EB-like event to which we refer.

Comparison of the inverted maps to the original undegraded parameters directly in the simulations[12] reveals that the atmospheric parameters are qualitatively well-retrieved. However, a careful quantitative comparison with the corresponding original maps at $\log\tau = -1$ reveals that the retrieved field strength and LOS velocities turn out to be strongly underestimated. This is a consequence of two effects. First, these inversions assume that these parameters are constant with height, which, as a result, gives a value that is an average of the height profile of an atmospheric parameter-weighted appropriate response function of the spectral line (Borrero et al. 2014). Second, both magnetic field strength and velocity change rapidly with height, especially in this run, which starts with a specific magnetic field setup. Also, the retrieved temperature at $\log\tau = -2.5$ resembles more closely the original temperature at $\log\tau = -1.5$, than the one at the same optical depth. The difference is too large to be attributed simply to spatial degradation. Again, this might simply be a characteristic of this particular run, with strong field emergences over the whole simulation domain and atmospheric stratification that is somewhat different from the canonical model atmospheres.

Simulations show a scenario similar to the observations. An EB-like event is produced as the footpoints of two newly emerging flux concentrations come into contact. The difference is that this particular simulated EB-like feature changes in brightness; it dims and then brightens up again as more flux approaches the cancellation point (at $t = 17.5$ minute and then again a minute later), while observations show a constant increase in the AIA 1700 brightness. This is directly related to upflows. They are persistent in observations, but shorter and intermittent in simulations. The simulated upflows develop first at [11″, 3.″5], already before $t = 15.1$ minutes, and then again at [6″, 3.″5] at $t = 15.9$ minutes.

[12] Also provided at http://www2.mps.mpg.de/data/outgoing/danilovic/ebs/.

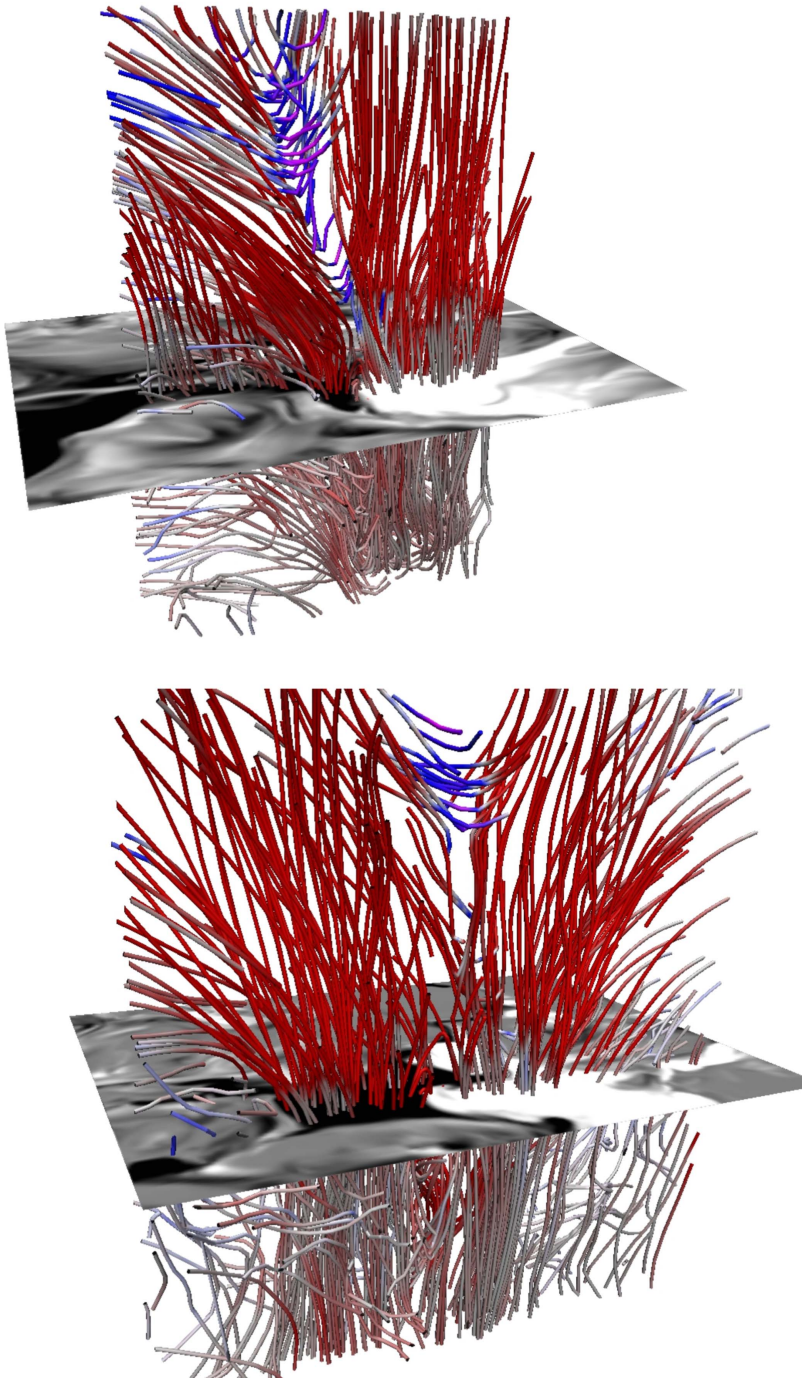

Figure 4. Magnetic field lines at two time instances: $t = 17.5$ minute (top panel) and $t = 25.8$ minute (bottom panel). The color coding corresponds to the vertical velocity with upflows being blue.

Although the observed event seems to be more dynamic and violent, as it produces faster flows and higher temperatures, qualitative similarities with simulations can be found. First, as shown in Section 2, we find one prominent case of a temperature increase at the footpoint of an emerging loop in the observations. Because emergence takes place over the whole simulation domain in simulations, similar features can be found in more than one location, as is evident in Figure 6 e.g., at $t = 19$ minutes. These hot spots coincide mostly with edges of elongated granule, but can appear as "islands" in intergranular lanes, e.g., at [11″, 5″] at $t = 25.8$ minutes. At these pixels, the inversion code retrieves temperature increase at all three nodes, the same way as in the case of observations. Cuts through two examples marked by vertical lines in Figures 5 and 6 are displayed in Figure 7. The cuts show fast downflows and strongly shifted optical depth scale at these locations. In the top case, no opposite polarity is present, as it is in most of these hot spots. Sometimes, as the second example illustrates, opposite polarities do come into contact near the optical depth unity, and the temperature is then additionally increased by Ohmic heating. None of these hot spots are connected in any direct way to the EB-like event.

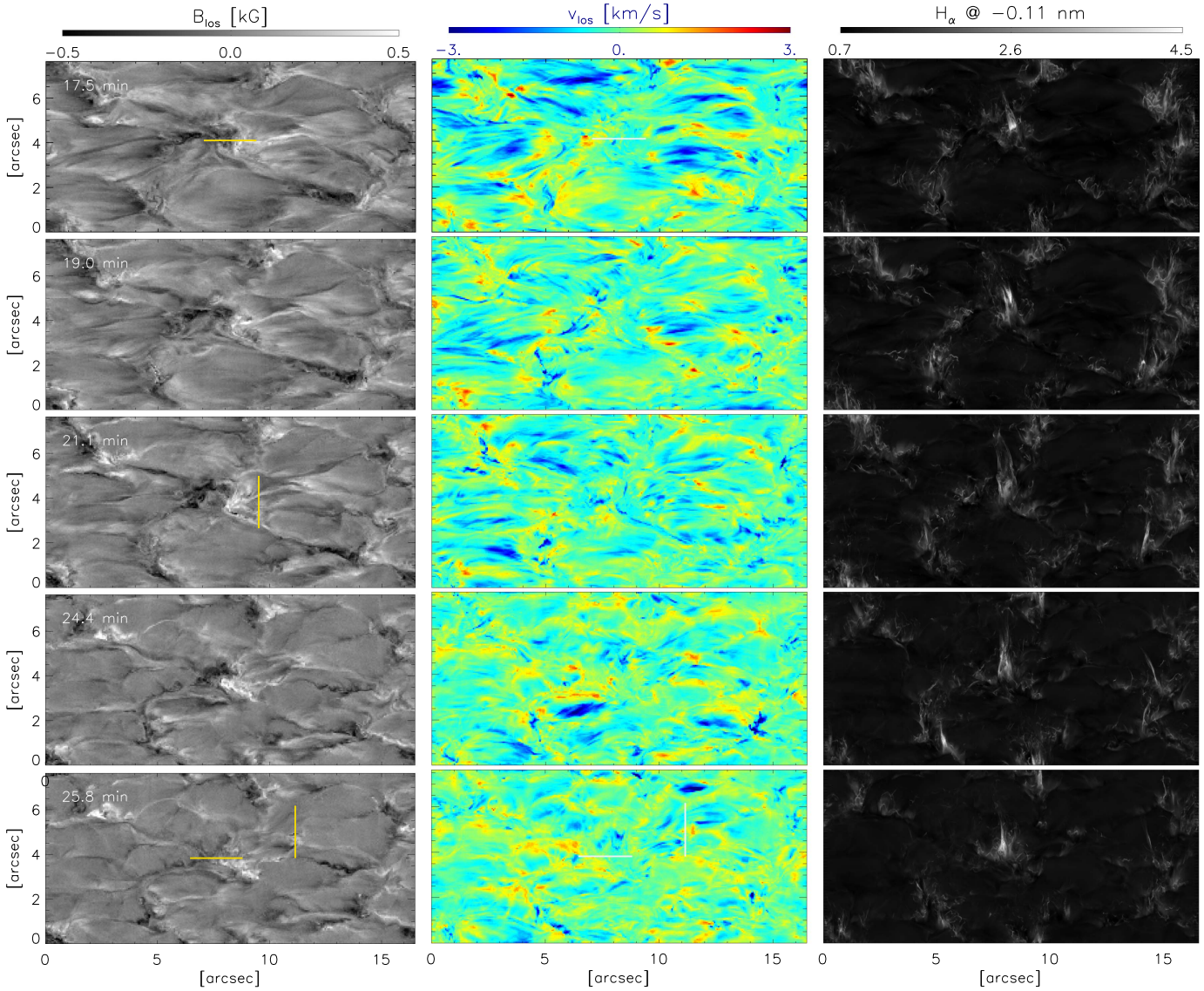

Figure 5. Simulated SUNRISE/IMaX observations—LOS magnetic field strength and LOS velocity (upflows are colored blue) obtained from inversions of the simulations at five different times during the evolution of the simulated EB-like event. Vertical/horizontal lines mark the position of the cuts shown in Figures 7 and 8. The rightmost column shows the Hα-wing images synthesized from the same snapshots. Bright flame-like features mark the positions of the simulated EBs.

The second similarity with observations can be found at the neutral line between the opposite polarities. Although the onset of the simulated EB-like event starts already at $t = 17.5$ minutes, inverted temperature maps show a temperature increase at this location only in the next snapshot, some 30 s later. Identically to our observations, after it is retrieved at the top node, similar signatures can also be found in the lower nodes. The largest jump in the temperature is always retrieved at the highest node in both simulations and observations. We choose to examine simulated parameters in more detail in Figure 8, at two instances where inversions give different stratifications. At the first moment, the inversions give regular temperature profile; in the second, a temperature increase at all nodes is retrieved.

Figure 8 shows the neutral line situated vertically in the middle of the plots, where magnetic field strength has a minimum. The thin signature in temperature outlines where the current density, and hence the Ohmic heating, is the largest. Contours outline the region where the contribution function to the line depression at the line's nominal wavelength position reaches 99% of its maximum value. These are the same instances shown also in Figure 4.

In the first instance (top panel in Figure 8), the reconnection already started and temperature is already increased by more than 2500 K at 200 km above the surface. Because of this large temperature jump, the formation of the Fe I 525.02 nm line is cut off at that height, so the line sees only the part of the atmosphere where the temperatures shows no significant changes. With time, the jump in the temperature moves downward, so that by $t = 25.8$ minutes, temperature reversal happens close to the the surface. From a relatively normal value there, the temperature gradually increases until it reaches a maximum of 9000 K at a height of around 500 km. In this case, the Fe I 525.02 nm line is formed very close to the surface and samples a very shallow layer of less than 50 km in height. The retrieved temperatures are still significantly underestimated even at those heights, which could be a consequence of the spatial degradation.

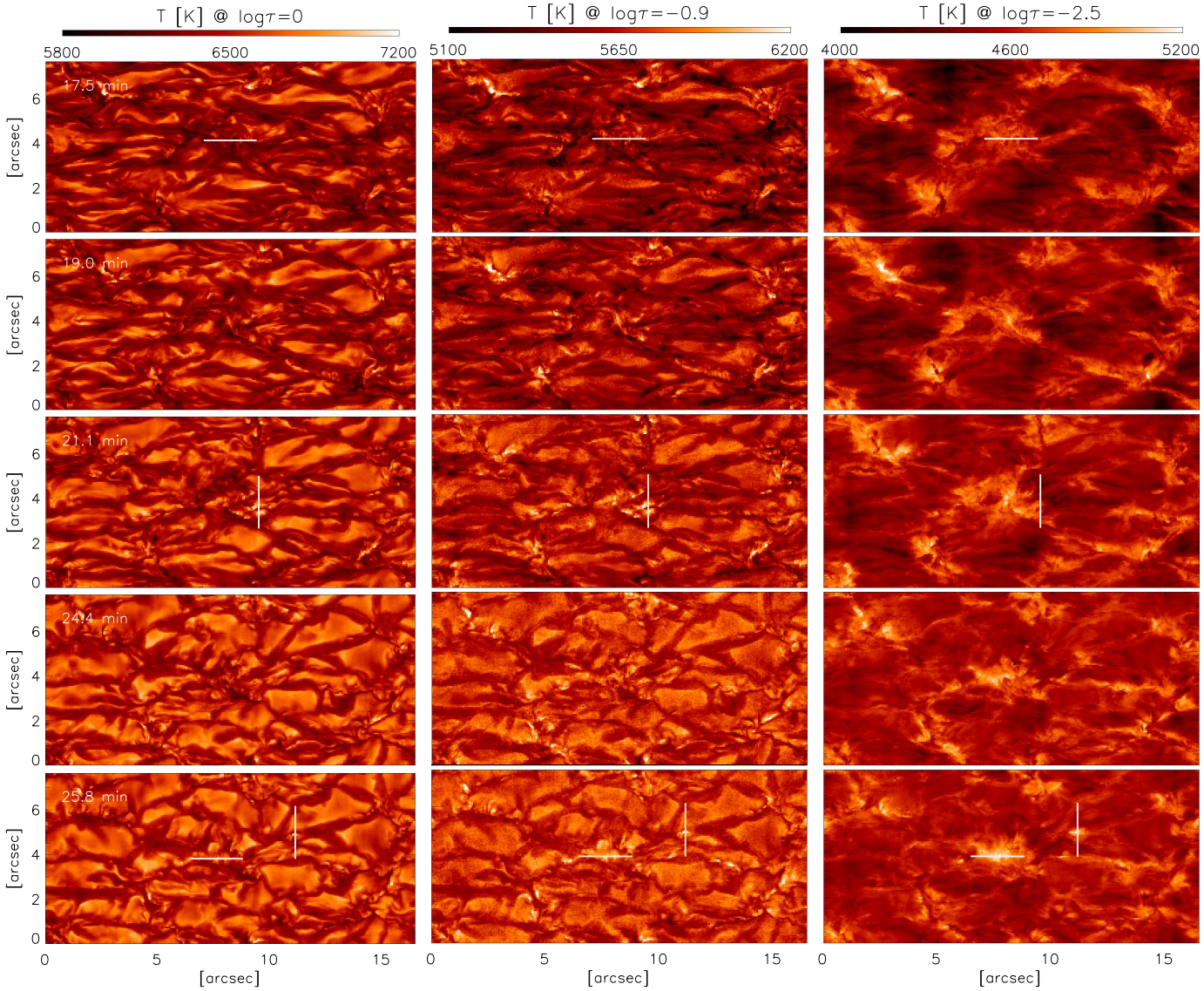

Figure 6. Simulated SUNRISE/IMaX observations—temperatures at $\log\tau = 0$, -0.9 and -2.5 retrieved by the inversions at the same times as in Figure 5. Vertical/horizontal lines mark the position of the cuts shown in Figures 7 and 8.

4. Conclusions

During the evolution of NOAA AR 11768, an event at the confluence of two flux emergences produced a significant brightness increase in the SDO/AIA 1700 channel. Given that AIA 1700 brightness was above the 5σ threshold set by Vissers et al. (2013), we claim that this event can be classified as an EB. This claim is further reinforced by the underlying field configuration recovered by Centeno et al. (2017). They demonstrate that the event was produced during subsequent appearance of two emerging flux regions where the field is aligned in a way that points to a serpentine-like field topology. Observations strongly suggest that this is an environment where EBs inevitably appear (Georgoulis et al. 2002; Pariat et al. 2004, 2006).

In this work, we analyze in detail photospheric signatures of the event recorded by SUNRISE/IMaX. We compare the results with a numerical experiment that reproduces the proposed flux emergence scenario. The simulated event results in a temperature increase that is in agreement with previous EB models (Fang et al. 2006; Bello González et al. 2013; Berlicki & Heinzel 2014; Hong et al. 2014) and produces the typically observed morphology of EBs in the wings of Hα.

Simulations show the expected field topology at the onset of the EB-like feature. The reconnection seems to start in the photosphere, some 200 km above the surface. As new material and fresh magnetic flux emerges, the current sheet between the two opposite polarities of the two emerging features extends further up, and the location where post-reconnection U-loops begin is shifted to above 1 Mm. During the whole evolution, no actual information on the location where the reconnection takes place is contained in the Fe I 525.02 nm line. As the energy is deposited in the upper photosphere, there the temperature rapidly changes and then is modified further down by the reconnection aftermath, e.g., downward propagating reconnection jets, as they collide with the local plasma. Because of this, the formation height of Fe I 525.02 nm line is continually

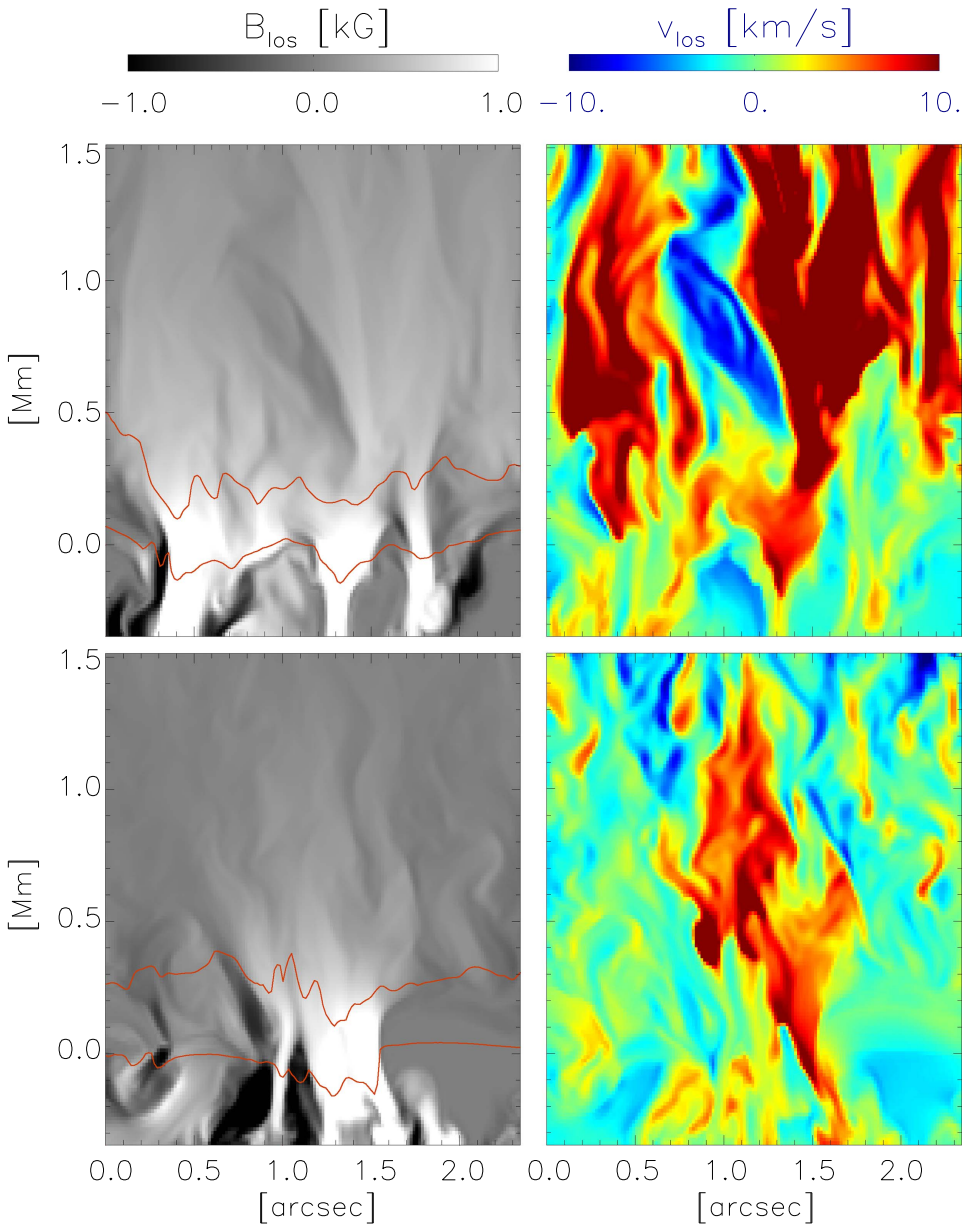

Figure 7. Vertical cuts over locations marked by vertical lines in Figures 5 and 6 show the LOS component of the magnetic field (left) and LOS velocity (right; upflows are colored blue). The $\log\tau = 0$ and $\log\tau = -2$ levels are outlined by red lines.

shifted downward until the moment when the line samples only a very shallow layer near the solar surface. This is in agreement with observations suggesting that these events produce sufficient energy to ionize the neutral metals (Rutten et al. 2015) and explains the very low temperature increase found by Reid et al. (2016).

Simulations suggest that not all locations where temperature increases are necessarily related to the event itself. Some of those appear at the footpoints of rapidly emerging loops as they expand in the horizontal direction upon reaching the surface. While material is drained, the footpoints are squeezed between already developed magnetic features and fast-moving emerging material. As a result, fast downflows are generated and footpoints are quickly evacuated. These locations might be similar to the high-temperature points presented by Tortosa-Andreu & Moreno-Insertis (2009) and could have similar characteristics from slanted viewing angles, as was the case for the flows studied by Bellot Rubio (2009) and Vitas et al. (2011). They also resemble, in some ways, locations of convective collapse.

Although they show qualitative similarities with the observations, the simulations fail to produce equally high temperatures. Comparison of the field strength, and especially the velocities, highlights the fact that the choice of the initial magnetic field setup is not ideal. To produce an event that is as dynamic and violent as the observations suggest, more magnetic buoyancy is needed, to launch the magnetic field into the solar atmosphere more efficiently. Also, persistent upflows that last at least three times longer seem to be essential. For this, instead of an embedded thin flux sheet, one needs to insert into the simulation domain either more flux, or a flux sheet over an extended period of time.

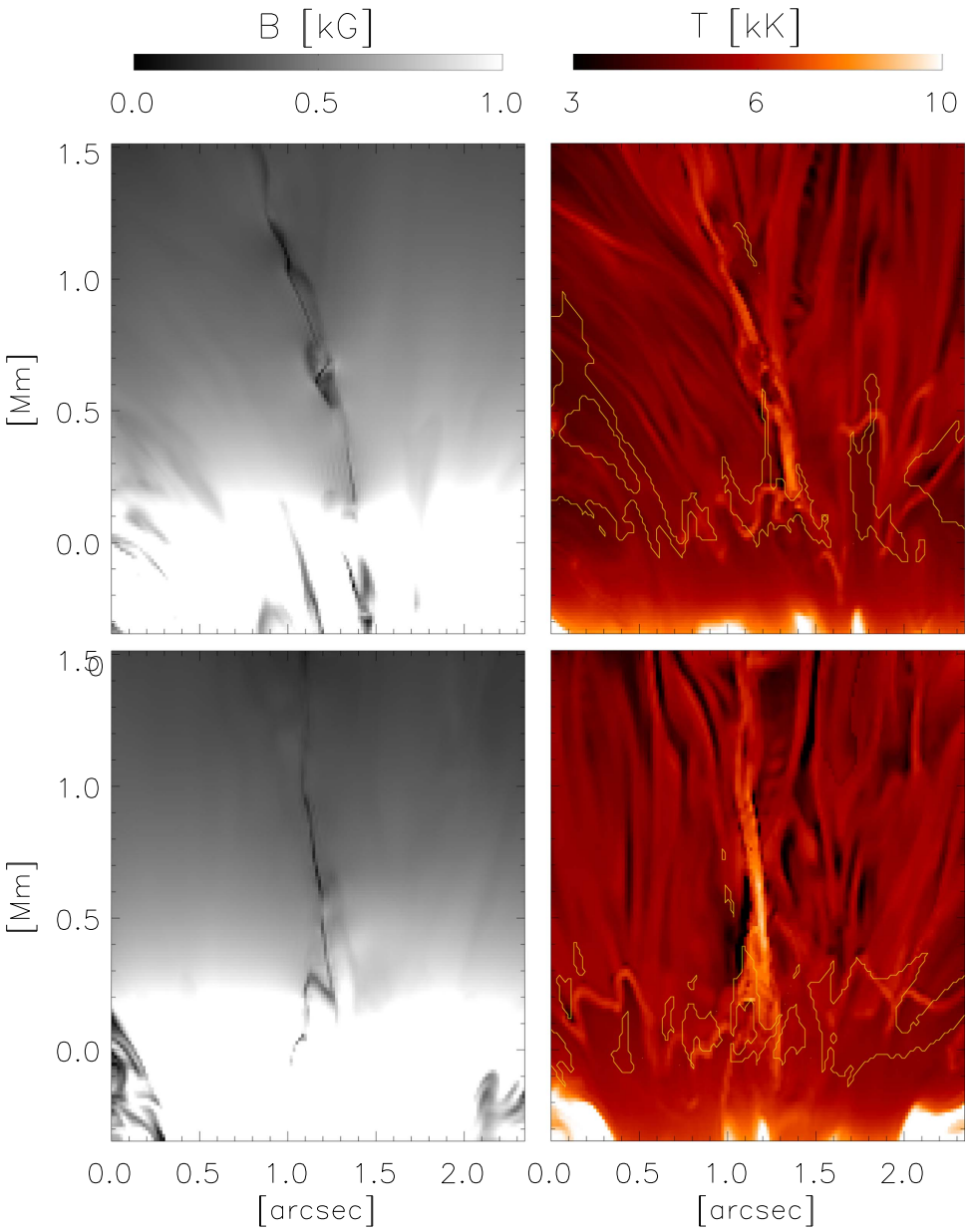

Figure 8. Vertical cuts over locations marked by the horizontal lines in Figures 5 and 6 show magnetic field strength and temperature at two instances during the evolution of the simulated EB-like event. Yellow contours show the formation height range of the Fe I 525.02 nm line. The same snapshots are also shown in Figure 4.

The German contribution to SUNRISE and its reflight was funded by the Max Planck Foundation, the Strategic Innovations Fund of the President of the Max Planck Society (MPG), DLR, and private donations by supporting members of the Max Planck Society, which are all gratefully acknowledged. This work has benefited from the discussions at the meeting "Solar UV bursts—a new insight to magnetic reconnection" at the International Space Science Institute (ISSI) in Bern. The Spanish contribution was funded by the Ministerio de Economia y Competitividad under Projects ESP2013-47349-C6 and ESP2014-56169-C6, partially using European FEDER funds. The HAO contribution was partly funded through NASA grant number NNX13AE95G. The National Solar Observatory (NSO) is operated by the Association of Universities for Research in Astronomy (AURA) Inc. under a cooperative agreement with the National Science Foundation. This work was also partly supported by the BK21 plus program through the National Research Foundation (NRF), funded by the Ministry of Education of Korea.

References

Archontis, V., & Hood, A. W. 2009, A&A, 508, 1469
Barthol, P., Gandorfer, A., Solanki, S. K., et al. 2011, SoPh, 268, 1
Bello González, N., Danilovic, S., & Kneer, F. 2013, A&A, 557, A102
Bellot Rubio, L. R. 2009, ApJ, 700, 284
Berkefeld, T., Schmidt, W., Soltau, D., et al. 2011, SoPh, 268, 103
Berlicki, A., & Heinzel, P. 2014, A&A, 567, A110
Borrero, J. M., Lites, B. W., Lagg, A., Rezaei, R., & Rempel, M. 2014, A&A, 572, A54
Centeno, R., Blanco Rodríguez, J., Solanki, S. K., et al. 2017, ApJS, 229, 3
Cheung, M. C. M., Schüssler, M., & Moreno-Insertis, F. 2007, A&A, 467, 703
Ellerman, F. 1917, ApJ, 46, 298
Fang, C., Tang, Y. H., Xu, Z., Ding, M. D., & Chen, P. F. 2006, ApJ, 643, 1325

Frutiger, C., Solanki, S. K., Fligge, M., & Bruls, J. H. M. J. 2000, A&A, 358, 1109
Gandorfer, A., Grauf, B., Barthol, P., et al. 2011, SoPh, 268, 35
Georgoulis, M. K., Rust, D. M., Bernasconi, P. N., & Schmieder, B. 2002, ApJ, 575, 506
Hashimoto, Y., Kitai, R., Ichimoto, K., et al. 2010, PASJ, 62, 879
Hong, J., Ding, M. D., Li, Y., Fang, C., & Cao, W. 2014, ApJ, 792, 13
Isobe, H., Tripathi, D., & Archontis, V. 2007, ApJL, 657, L53
Kitai, R. 1983, SoPh, 87, 135
Leenaarts, J., Rutten, R. J., Sütterlin, P., Carlsson, M., & Uitenbroek, H. 2006, A&A, 449, 1209
Lemen, J. R., Title, A. M., Akin, D. J., et al. 2012, SoPh, 275, 17
Martínez Pillet, V., del Toro Iniesta, J. C., Álvarez-Herrero, A., et al. 2011, A&A, 523, A111
Matsumoto, T., Kitai, R., Shibata, K., et al. 2008, PASJ, 60, 577
Nelson, C. J., Shelyag, S., Mathioudakis, M., et al. 2013, ApJ, 779, 125
Pariat, E., Aulanier, G., Schmieder, B., et al. 2004, ApJ, 614, 1099
Pariat, E., Aulanier, G., Schmieder, B., et al. 2006, AdSpR, 38, 902
Pesnell, W. D., Thompson, B. J., & Chamberlin, P. C. 2012, SoPh, 275, 3
Reid, A., Mathioudakis, M., Doyle, J. G., et al. 2017, ApJ, 823, 110
Rempel, M., Schüssler, M., & Knölker, M. 2009, ApJ, 691, 640
Rezaei, R., & Beck, C. 2015, A&A, 582, A104
Rutten, R. J. 2007, in The Physics of Chromospheric, Vol. 368, ed. P. Heinzel, I. Dorotovi, & R. J. Rutten (San Francisco, CA: ASP), 27
Rutten, R. J. 2016, A&A, 590, A124
Rutten, R. J., Rouppe van der Voort, L. H. M., & Vissers, G. J. M. 2015, ApJ, 808, 133
Rutten, R. J., van Veelen, B., & Sütterlin, P. 2008, SoPh, 251, 533
Rutten, R. J., Vissers, G. J. M., Rouppe van der Voort, L. H. M., Sütterlin, P., & Vitas, N. 2013, JPhCS, 440, 012007
Solanki, S. K., Barthol, P., Danilovic, S., et al. 2010, ApJL, 723, L127
Solanki, S. K., Riethmüller, T. L., Barthol, P., et al. 2017, ApJS, 229, 2
Tian, H., Xu, Z., He, J., & Madsen, C. 2016, ApJ, 824, 96
Tortosa-Andreu, A., & Moreno-Insertis, F. 2009, A&A, 507, 949
Vissers, G. J. M., Rouppe van der Voort, L. H. M., & Rutten, R. J. 2013, ApJ, 774, 32
Vissers, G. J. M., Rouppe van der Voort, L. H. M., Rutten, R. J., Carlsson, M., & De Pontieu, B. 2015, ApJ, 812, 11
Vitas, N., Fischer, C. E., Vögler, A., & Keller, C. U. 2011, A&A, 532, A110
Vögler, A., Shelyag, S., Schüssler, M., et al. 2005, A&A, 429, 335
Watanabe, H., Vissers, G., Kitai, R., Rouppe van der Voort, L., & Rutten, R. J. 2011, ApJ, 736, 71